Carbon 231 (2025) 119691

Contents lists available at ScienceDirect

Carbon

journal homepage: www.elsevier.com/locate/carbon

Boosting through-plane electrical conductivity: chitosan composite films with carbon-sepiolite and multiwalled carbon nanotubes

Ana Barra [a,b], Nuno M. Ferreira [c], Fátima Poças [d], Eduardo Ruiz-Hitzky [b], Cláudia Nunes [a,**], Paula Ferreira [a,*]

[a] CICECO – Aveiro Institute of Materials, Department of Materials & Ceramic Engineering, University of Aveiro, Aveiro, 3810-193, Portugal
[b] ICMM – Instituto de Ciencia de Materiales de Madrid, CSIC, c/ Sor Juana Inés de la Cruz 3, Madrid, 28049, Spain
[c] i3N, Department of Physics, University of Aveiro, 3810-193, Aveiro, Portugal
[d] Universidade Católica Portuguesa, CBQF - Centro de Biotecnologia e Química Fina – Laboratório Associado, Escola Superior de Biotecnologia, Rua Diogo Botelho 1327, 4169-005, Porto, Portugal

ARTICLE INFO

Keywords:
Biocomposite films
Chitosan
Carbon-sepiolite
Multiwalled carbon nanotubes
Electrical conductivity

ABSTRACT

Flexible and electrically conductive materials are gaining significant attention across various domains, notably in electronics, biomedicine and food industry. One promising strategy involves the integration of electrically conductive nanostructures into a polymeric matrix to fabricate composite materials. However, achieving uniform through-plane electrical conductivity remains a challenge due to the preferential alignment of carbon nanostructures in the in-plane direction. Herein, we report the development of electrically conductive chitosan (CS)-based biocomposite films incorporating a multicomponent filler system. By combining carbon supported on sepiolite clay (CARSEP) with multiwalled carbon nanotubes (MWCNT), it is aimed to facilitate an interconnected distribution in both in-plane and through-plane directions. The optimized film, featuring a CS/CARSEP/MWCNT mass ratio of 50/40/10, exhibited a maximum electrical conductivity of 55.5 S/m and 0.1 S/m in the in-plane and through-plane directions, respectively. Additionally, migration studies demonstrated the absence of harmful compounds upon heating the film up to 60 °C in air, ethanol, or hexane. These findings highlight the potential of these flexible and electrically conductive biocomposite films, primarily composed of biobased materials, for applications requiring through-plane electrical conductivity.

1. Introduction

Flexible and electrically conductive materials, such as the intrinsically conductive polymers, play a crucial role in several fields such as electronics, biomedical, and the food industry [1–3]. However, the poor processability, low solubility and lack of natural biodegradation can be drawbacks to their practical applications. The design of biocomposite materials using electrically conductive fillers is an alternative that offers the advantage of manipulating the physicochemical properties according to the requirements of the application [4–7].

The use of biopolymeric matrices is an ecological alternative that contributes to mitigate the environmental impact. Chitosan (CS) is a polycationic linear polysaccharide constituted by β-(1 → 4)-linked D-glucosamine (deacetylated unit) and N-acetyl-d-glucosamine (acetylated unit) [8,9]. This biopolymer is an attractive matrix considering its abundant, renewable nature, biodegradability and film forming ability. Recently it has been selected for cutting-edge applications such as implantable and bioresorbable electronic devices or edible electronics [10–13].

Flexible and electrically conductive materials are necessary for several other applications such as piezoresistive sensors, electromagnetic interference shielding or electrically conductive packaging [14–17]. Pulsed Electric Field (PEF) is a non-thermal food processing technology that consists into the application of short, high-voltage pulses to food products to inactivate enzymes and microorganisms [18]. Currently, PEF is performed in a treatment chamber before packaging, which presents food safety concerns due to risk of recontamination after sterilization. The PEF treatment in-pack, using a flexible electrically conductive packaging could eliminate recontamination risks [19].

* Corresponding author.
** Corresponding author.
E-mail addresses: claudianunes@ua.pt (C. Nunes), pcferreira@ua.pt (P. Ferreira).

https://doi.org/10.1016/j.carbon.2024.119691
Received 14 June 2024; Received in revised form 14 September 2024; Accepted 6 October 2024
Available online 9 October 2024

Carbon nanostructures such as reduced graphene oxide (rGO) and multiwalled carbon nanotubes (MWCNT) are fillers able to provide electrical conductivity to the insulator biopolymeric matrices [20–23]. In our previous work [24], electrically conductive chitosan-based composite films were prepared using rGO eco-friendly reduced by hydrothermal carbonization in presence of caffeic acid. The films showed an electrical conductivity of 0.7 S/m and 2.1×10^{-5} S/m in-plane and through-plane direction, respectively [24]. Similarly, starch films containing rGO obtained by hydrothermal reduction (25 % w/w of dry polysaccharide weight) presented an electrical conductivity of 6.5×10^{-3} S/m in-plane and 2.9×10^{-6} S/m through-plane direction [25]. The rGO produced using mild reducing methods presents lower electrical conductivity than rGO obtained by stronger reducing agents. Nevertheless, the reduction method is not a critical parameter to overcome the discrepancy between the electrical conductivity in both directions. Polyurethane composites with 4 wt% rGO in situ reduced by hydrazine presented electrical conductivities of 0.1 S/m (in-plane) and 1.7×10^{-6} S/m (through-plane). The difference between the in-plane and through-plane electrical conductivity is attributed to the preferential self-alignment of rGO sheets in-plane direction, resulting in anisotropic electrically conductive materials [26]. The use of carbon nanostructures with a different morphology, such as MWCNT, produced a similar outcome. Starch films containing 5% MWCNT dispersed with the surfactant sodium dodecyl sulphate (SDS) showed an electrical conductivity of 6.2 S/m (in-plane) and 1.5×10^{-5} S/m (through-plane), suggesting a random orientation of MWCNT in-plane direction [25]. Therefore, the improvement of the through-plane electrical conductivity is challenging.

The through-plane electrical conductivity of composites containing MWCNT can be accomplished by their alignment in this direction. The vertical alignment of MWCNT can be performed by several methods, for example using the electric or magnetic fields [27,28]. However, these methods are complex and expensive, thus incompatible with large-scale production of composites. The combination of carbon nanostructures with different morphology, their use in high loads and the improvement of the dispersion can establish an interconnected 3-dimensional (3D) percolation network [29,30]. Alginate-based biocomposite films containing 55.6% graphene nanoplatelets (GNP) and 10 % MWCNT displayed an enhanced through-plane electrical conductivity in the range of 10^{-2} S/m. This result was accomplished not only due to the high load of highly electrically conductive GNP and MWCNT fillers, but also due to their improved dispersion using sepiolite (SEP), a clay mineral [31]. SEP is a natural Mg-silicate of micro/nano-fibrous morphology with a crystalline structure alternating in blocks and tunnels of nanometer section extending along the fiber axis and exhibiting a large specific surface area and a high density of surface silanol groups (≡Si–OH) [32,33]. These characteristics, together with its unique rheological properties, allow its assembly to a wide range of organic and inorganic substances generating functional materials with wide applications [33–35]. In this context, SEP has been extensively used for the preparation of diverse polymer-composite materials, including chitosan (CS)-based bionanocomposites [36].

SEP can also be used as support for the formation of graphene-like carbon from natural precursors. Sucrose, liquid caramel, or gelatin were impregnated into SEP followed by pyrolysis at 800 °C for 1 h under inert atmosphere [37,38]. The resulting carbon-sepiolite (CARSEP) hybrid nanocomposites are constituted by aggregated sepiolite fibers covered and bounded by carbon, with an electrical conductivity in the range of 1–100 S/m. These CARSEP hybrids are good candidates to be used as fillers in polymer composites [39].

In this work, we designed a flexible CS-based composite film, using mainly natural precursors, with high in-plane electrical conductivity to be applied in several fields. Liquid caramel and natural SEP clay were used as precursors to obtain the CARSEP hybrid nanocomposite, that along with MWCNT were used as a multicomponent filler system. The structure, morphology, and thermal stability of films was studied. The effect of fillers ratio on the water solubility and swelling, wettability, mechanical properties, and electrical conductivity was also investigated. To evaluate the safety of the film, a migration study was performed on the most promising film after being heated up to 60 °C in contact with air, ethanol, and hexane.

2. Experimental section

2.1. Chemicals

SEP clay (Pangel® S9), a very pure rheological grade Mg-silicate from the Taxus Basin deposits was supplied by Tolsa S.A. (Madrid, Spain). CS (Sigma-Aldrich, medium molecular weight, deacetylation ≥75%), MWCNT with average diameter of 10 nm and average length of 1–2 μm were supplied by Dropsens (Oviedo, Spain). Acetic acid (99–100%, p. a.) was supplied by LabChem. Glycerol (99.5% Scharlau). Commercial liquid caramel was supplied by Kraft.

2.2. Synthesis of carbon-sepiolite filler

The CARSEP filler was synthesized following the procedure described by Ruiz-García et al. [40] with some adaptations, Fig. 1A. Briefly, SEP and commercial liquid caramel (1:4) were mixed in water using a spatula following ultrasonic homogenization (6 kJ/40 mL) to obtain the CARSEP precursor. The mixture was dried at 105 °C for 48 h for water evaporation. The pyrolysis was performed in a tube furnace (Carbolite, Derbyshire, England) at 800 °C with a heating rate of 5 °C/min and a residence time of 1 h under an inert N_2 atmosphere. The obtained material, CARSEP filler, was grinded to powder using a batch mill (IKA A10 basic, Germany) and sieved using a 75 μm mesh sieve.

2.3. Preparation of biocomposite films

The biocomposite films were prepared according to the scheme depicted in Fig. 1B. A suspension of carbonaceous fillers was obtained by the ultrasonic dispersion of CARSEP and MWCNT (Table 1) in water using the ultrasounds probe (19 kJ/100 mL). Then, acetic acid was added to the fillers dispersion to obtain a 0.1 M solution. CS (Table 1) was added to the solution and kept under magnetic stirring overnight at room temperature to dissolve and homogenize with the fillers. The solution was filtered using a nylon mesh cloth to remove undissolved CS impurities. Glycerol, 50% in relation to chitosan mass, was added and the suspension was maintained at 50 °C for 10 min to promote glycerol homogenization. The biocomposite films were prepared by solvent casting, according to the method previously reported with some modifications [24]. The biocomposite suspensions (26 g) were transferred to acrylic casting molds with 6×6 cm^2 and maintained at 35 °C overnight for solvent evaporation. The nomenclature attributed to the biocomposite films stands for its composition, Tables 1 and *ie.*, wt% CS/CARSEP/MWCNT: 100/0/0, 50/50/0, 50/45/5, and 50/40/10.

2.4. Characterization methods

X-ray diffraction (XRD) of starting materials and films was performed with a Panalytical X'Pert PRO3 diffractometer at 45 kV 40 mA using Cu target Kα radiation. The diffraction patterns were acquired from 3 to 100°, with a 0.01° step size and 50 s per step.

Specific surface area of SEP and CARSEP precursors were obtained from −196 °C N_2 adsorption-desorption isotherms using a Micromeritics ASAP 2010 equipment.

Solid-state carbon-13 cross-polarization magic angle spinning nuclear magnetic resonance (^{13}C CP MAS-NMR) spectra of CARSEP precursor and CARSEP filler were recorded in a Bruker Avance 400 spectrometer, using an external magnetic field of 9.4 T. 1-Dimensional (1D) spectra were taken at room temperature, while the samples were spinning at 10 kHz around the magic angle (54°44′ with respect to the

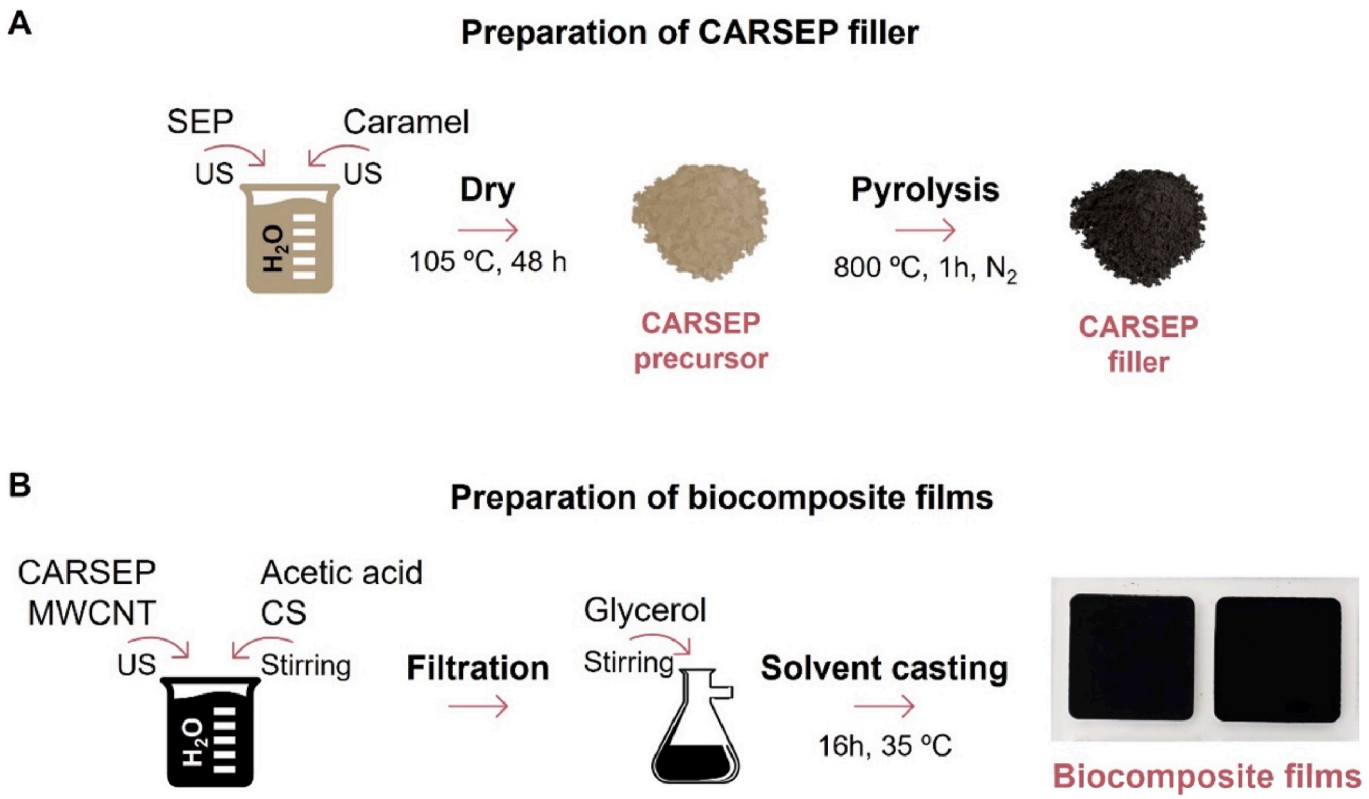

Fig. 1. Schematic representation of the preparation of (**A**) CARSEP filler and (**B**) biocomposite films.

Table 1
Composition of biocomposite films presented in terms of wt% of CS matrix and CARSEP and MWCNT fillers. Average thickness of samples. Different superscript letters (a, b) indicate statistical differences, $p < 0.05$.

Biocomposite	CS [wt%]	CARSEP [wt%]	MWCNT [wt%]	Thickness [μm]
100/0/0	100	0	0	146 ± 14^{a}
50/50/0	50	50	0	120 ± 13^{b}
50/45/5	50	45	5	$134 \pm 10^{a,b}$
50/40/10	50	40	10	140 ± 3^{a}

direction of the magnetic field) with a standard cross-polarization pulse sequence. Spectrometer frequencies were set to 100.62 and 400.13 MHz for ^{13}C and ^{1}H respectively. A contact time of 2 ms and a period between successive accumulations of 5 s were used to minimize saturation effects. The number of scans was 12000. Chemical shift values were referenced to tetramethyl silane (TMS).

Elemental chemical composition (CHN) of CARSEP precursor and CARSEP filler was determined by elemental analysis using a PerkinElmer 2400 Series II analyser.

Raman spectroscopy was carried out using a ProRaman-L spectrometer (ChemLogix) at room temperature. The spectra were generated using a 532 nm wavelength excitation laser.

Thermogravimetric analysis - differential scanning calorimetry (TGA-DSC) analysis of CARSEP precursor, CARSEP filler, and films were carried out from room temperature to 900 °C (10 °C/min) under N_2 flow using a SDT Q600 V20.9 Build 20 thermal gravimetric analyzer (TA Instruments, New Castle, DE, USA).

Field emission scanning electron microscopy (FESEM) analysis of films was performed using a Nova NanoSEM 230 microscope (FEI) at 5 kV acceleration voltage. Biocomposite films were attached to carbon tape for direct observation without the requirement of any conductive coating on their surface.

Mechanical properties of biocomposite films were studied by tensile tests according to the standard method ASTM D 882-83 using a texture analyzer (TA.XTplusC, Stable Micro Systems) equipped with a 5 kg loading cell. The films were cut into 6 × 1 cm^2 stripes. The grips were initially separated by 3 cm and the films were stretched at a constant rate of 0.5 mm/s until rupture. The films were stored inside a controlled moisture chamber, with a relative humidity of 45% for six days prior to the analysis. The thickness of each specimen was measured in six different points using a micrometer (Mitutoyo Corporation). Six specimens per type of film were analyzed.

Water contact angle (WCA) of films was measured using an optical contact angle system (Dataphysics). The contact angles between ultrapure water (3 μL drop) and the top or bottom surfaces of biocomposite films were determined by the Laplace - Young method. The films were stored inside a controlled moisture chamber, with a relative humidity of 45% for six days prior to the analysis. Ten contact angle values were considered for each sample.

Water swelling of films was investigated by immersing a piece of film in water for 24 h. The excess of water was removed with absorbent paper. The swelling percentage was calculated using Equation (1):

$$Swelling\ [\%] = \frac{(Ms - Md)}{Md} \times 100 \qquad \text{Equation 1}$$

Where Ms is the mass of film in swollen state and Md in dry state before immersion in the water.

Moisture and solubility of films were determined by their weight loss percentage. Specimens of films with 4 cm^2 were weighted, dried at 105 °C during 24 h and cooled down to room temperature inside a desiccator prior to final weight. The moisture was determined by Equation (2):

$$Moisture\ [\%] = \frac{(mi - mf)}{mi} \times 100 \qquad \text{Equation 2}$$

Where *mi* and *mf* stand for initial and final mass, respectively.

The solubility was determined by the weight loss percentage upon

immersion of films in water for 7 days under constant stirring at 80 rpm. The specimens of films (4 cm^2) were weighted before and after the essay. In the latter case, the films were dried and cooled down to room temperature using the same conditions described above. The solubility was determined using Equation (3):

$$Solubility\ [\%] = \frac{(mi - mf)}{mi} \times 100 \quad \text{Equation 3}$$

Where *mi* and *mf* stand for initial mass and final mass, respectively. The initial mass was corrected for the mass of the dry film considering the percentage of moisture. Three specimens per type of film were analyzed.

Electrical conductivity of films was measured in-plane and through-plane directions by direct current (*dc*) measurements using a power supply 72–2545 (TENMA) and two multimeters (DMM 6500, Keithley). The in-plane measurements were performed with four points probe resistivity setup using samples with 3.5 × 0.5 cm^2. The through-plane measurements were performed with two points probe resistivity setup and samples with 1 cm^2. The electrical conductivity was determined using Equation (4) and Equation (5):

$$R = \frac{V}{I} \quad \text{Equation 4}$$

$$\sigma = \frac{L}{R \times S} \quad \text{Equation 5}$$

where the standard parameters for electrical circuits were used: R – resistance, V – tension, I – current, σ – electrical conductivity, L – length of the sample, S – cross sectional area of sample.

Migration studies were performed by gas chromatography coupled with mass spectrometry (GC-MS). Head space analysis: the sample was heated in a closed vial for 1 h at 60 °C. Chromatographic conditions: Column Zebron 5 MS (30 m × 0.25 mm (internal diameter) × 0.25 μm). Headspace injection volume 1 mL (split 1:10), injection temperature: 250 °C, oven temperature: 40 °C (5 min), 10 °C/min, 320 °C (2 min). MS TQ SCION: EI 70 eV Full Scan 33–350 *m/z*. Liquid extracts: the samples (6 cm^2) were extracted in ethanol or hexane (10 mL) for 1 h at 60 °C. The extracts were directly injected or after concentration 10 times by solvent evaporation under nitrogen flow. Chromatographic conditions: Column Zebron 5 MS (30 m × 0.25 mm (internal diameter) × 0.25 μm). Injection volume 1 μl (splitless 0.75 min), injection temperature: 50 °C during 3 min, followed by 320 °C during 15 min with a heating rate of 10 °C/min. Triple quadrupole GC-MS (SCION) with an electron ionization of 70 eV and full scan 33–700 *m/z* was used.

Statistical data treatment of moisture, solubility, swelling, water contact angle, thickness, mechanical and electrical properties were performed using the One-Way Analysis of Variance (ANOVA) with a significance level of 0.05 followed by the Tukey test using the OriginPro 2021 software.

3. Results and discussion

Fig. 1A and B show, respectively, the preparation of CARSEP filler and of the biocomposite films. In brief, the sequential ultrasounds (US) dispersion of SEP and liquid caramel in water was followed by a drying step to obtain the CARSEP precursor. The CARSEP filler was obtained by pyrolysis of CARSEP precursor, to transform the caramel into a carbonaceous material. SEP, used as a porous support for the formation of carbon, was maintained after pyrolysis. The biocomposite suspension was prepared by ultrasonic dispersion of carbonaceous fillers, CARSEP and MWCNT, in distilled water followed by the addition of the biopolymeric matrix. The suspension was filtered, with subsequent homogenization of glycerol used as plasticized. The biocomposite films were obtained by a simple solvent casting method. The effect of the fillers on the structure, morphology, and physical properties of biocomposite films was investigated.

3.1. Structural characterization

The crystalline structure of SEP, CARSEP precursor, CARSEP filler, and biocomposite films was evaluated by XRD, Fig. 2. The most intense reflections of SEP were preserved after the impregnation of liquid caramel, as observed in the diffraction pattern of CARSEP precursor [41]. Although, a decrease in peaks intensity was observed, suggesting the modification of fibers orientation probably due to interactions with caramel [42]. Caramel is expected to be located in the micropores of SEP and covering its surface, which is corroborated by the reduction of the specific surface area of CARSEP precursor (1 $m^2\ g^{-1}$) in comparison to SEP (337 $m^2\ g^{-1}$). The diffractogram of CARSEP filler shows a loss of crystallinity in comparison with CARSEP precursor, which can be ascribed to structural changes that take place during pyrolysis at 800 °C. Other studies in literature report shortening of SEP fibers and irreversible elimination of coordinated water molecules when SEP impregnated with polyacrylonitrile is subject to thermal treatment [43]. CS diffractogram presents two low intensity broad bands at $2\theta = 9.2°$ and $2\theta = 19.5°$, assigned to the (020) and (110) reflections, respectively [44]. The diffraction patterns of biocomposite films are similar to the diffraction pattern of CS, as a result of the low crystallinity of the major constituents, CS and CARSEP filler. The amorphous structure of CS was not affected by the incorporation of fillers. The same absence of crystallinity modifications was observed in biocomposites of CS and GO, which suggests a good homogenization between matrix and fillers [45].

The structural characterization of CARSEP precursor and CARSEP filler by solid-state ^{13}C *CP MAS-NMR* is shown in Fig. 3A. CARSEP precursor spectrum displays a signal centered at 71 ppm, attributed to carbons of glucose and fructose present in caramel used as precursor [46,47]. This signal disappears in CARSEP filler spectrum, being only observed a band centered at 122 ppm, which is typical of aromatic sp^2 carbons [38]. This result supports the conversion of caramel into graphitic carbon after the pyrolysis at 800 °C. The chemical composition of CARSEP precursor (36.1% C and 5.3% H) and CARSEP filler (53.0% C and 0.73% H) also reflects the increase of carbon content and reduction of hydrogen after the thermal treatment. Additionally, the graphitization of caramel is confirmed by the D (1334 cm^{-1}) and G (1583 cm^{-1}) graphitic bands present in the Raman spectrum of CARSEP filler (Fig. 3B) [48]. Raman spectroscopy of biocomposites was also performed to investigate if the fingerprint of graphitic materials is retained after blending CARSEP and MWCNT fillers with CS, Fig. 3B. 50/50/0

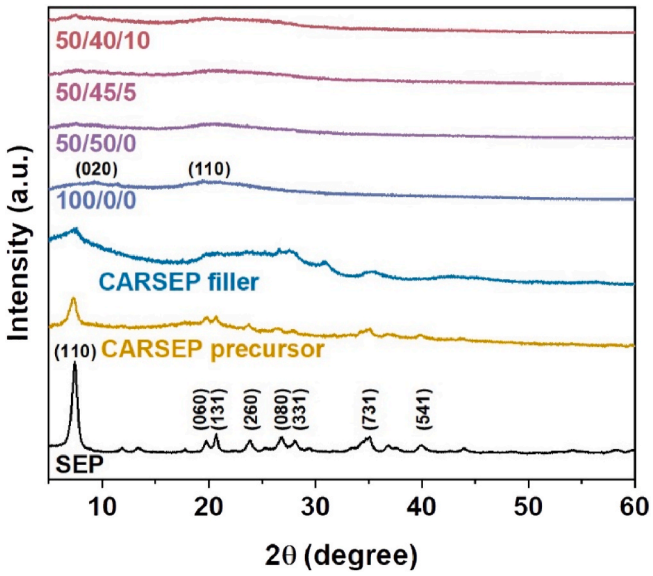

Fig. 2. XRD diffraction patterns of SEP, CARSEP precursor, CARSEP filler and 100/0/0, 50/50/0, 50/45/5, and 50/40/10 biocomposites.

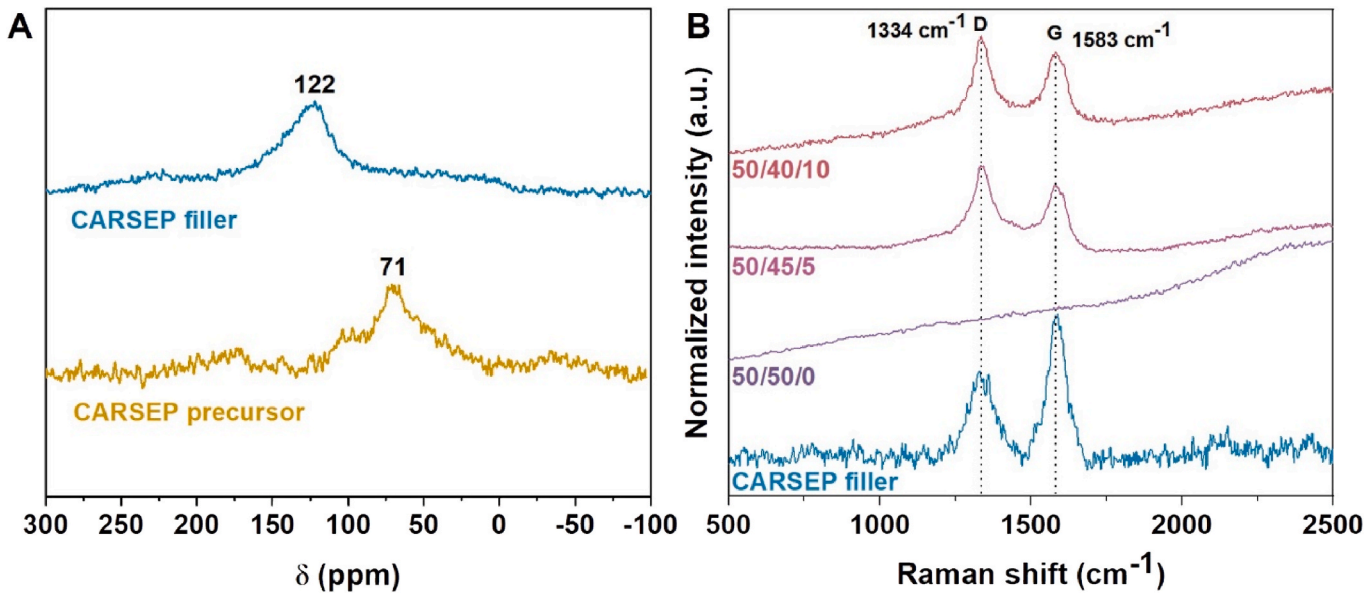

Fig. 3. (A) Solid-state ^{13}C *CP MAS-NMR* spectra of CARSEP precursor and CARSEP filler. (**B**) Raman spectra of CARSEP filler and 50/50/0, 50/45/5, and 50/40/10 biocomposites.

film spectrum does not display the D and G graphitic bands, suggesting a film surface predominantly covered by CS. However, the bands are observed in the spectra of 50/45/5 and 50/40/10 biocomposites, which should be due to the presence of MWCNT that also display the graphitic bands at the same wavelength [31].

3.2. Thermal analysis

The thermal stability of CARSEP precursor, CARSEP filler, 100/0/0, 50/50/0, 50/45/5, and 50/40/10 biocomposites was investigated by TGA (Fig. 4A) and DSC (Fig. 4B). The TGA profile of CARSEP precursor

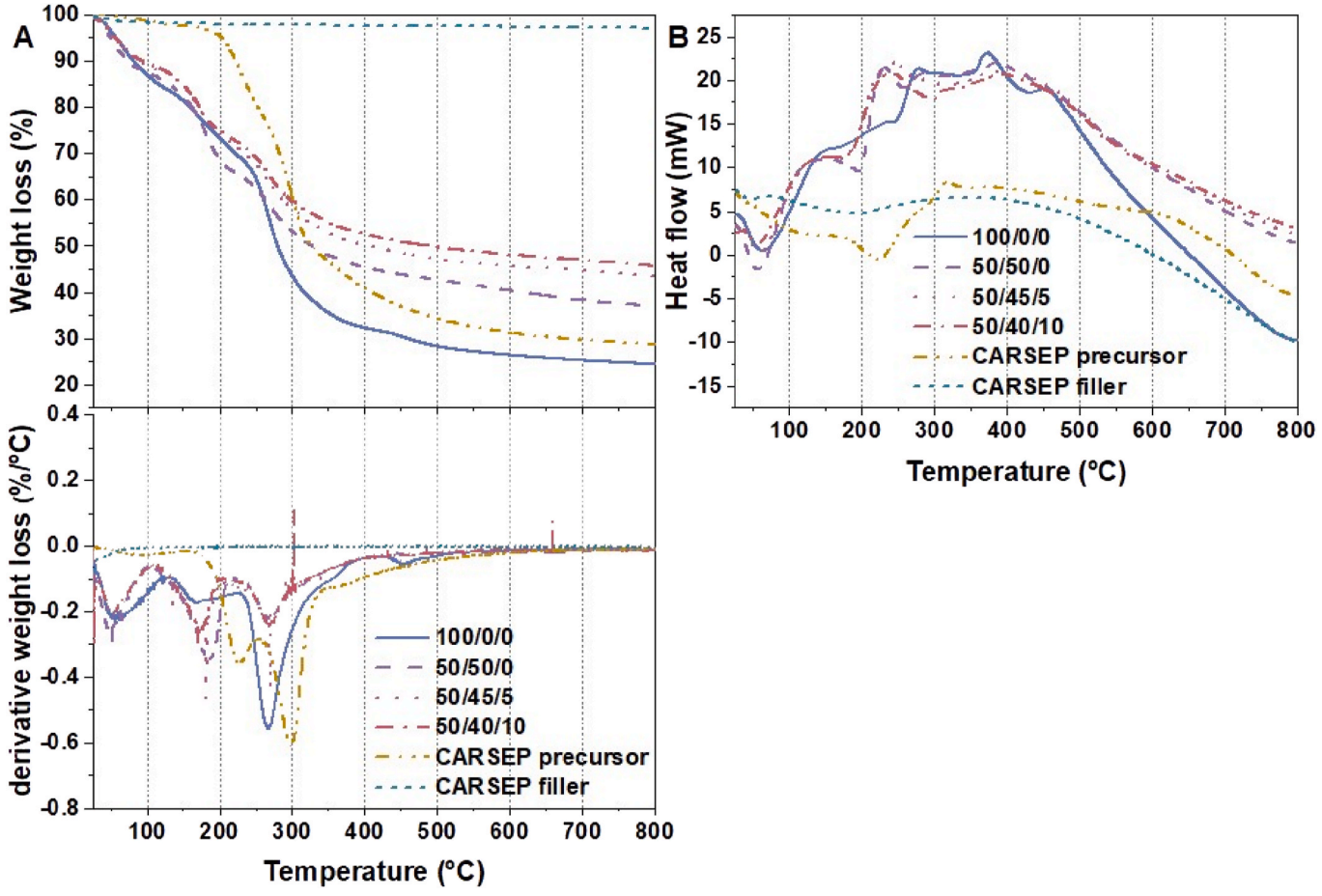

Fig. 4. (**A**) TGA and derivative TGA curves and (**B**) DSC curves of CARSEP precursor, CARSEP filler and biocomposite films.

shows a major weight loss between 180 and 320 °C, ascribed to the release of volatile compounds from caramel, which is followed by smaller weight losses related to the conversion of caramel into a carbonaceous material, losing a total of 73% weight until 900 °C. The CARSEP filler is thermally stable, losing less than 3% weight until 100 °C. This small weight loss is only ascribed to physically adsorbed water molecules, since the thermal decomposition previously took place during pyrolysis at 800 °C. The 100/0/0 film loses weight in three major steps. The first step, between 25 and 103 °C, corresponds to the evaporation of water physically adsorbed to CS. The second step, between 103 and 240 °C, is mainly attributed to glycerol degradation, but also to the release of water bonded to CS through hydrogen bonds. The third step, between 240 and 400 °C, is where the highest weight loss occurs, corresponding to the thermal degradation of CS molecules through chain depolymerization, decomposition of pyranose rings and ring opening reactions [49,50]. The 50/50/0, 50/45/5 and 50/40/10 biocomposites also lose weight in three steps similar to 100/0/0 film. However, the weight losses are smaller, as consequence of thermal stability of CARSEP and MWCNT fillers. The 100/0/0 film loses 77% of total weight, while 50/50/0, 50/45/5, and 50/40/10 biocomposites lose 65, 58 and 56%, respectively. These results indicate an improved thermal stability of biocomposites in comparison to 100/0/0 film, which is conferred by CARSEP filler and reinforced by MWCNT that are thermally stable carbonaceous materials.

The DSC curve of the 100/0/0 film shows an endothermic peak at approximately 62 °C, which is attributed to moisture loss. The glass transition temperature (T_g) is observed at 167 °C, while peaks appearing above 200 °C are associated with thermal decomposition of CS. The 50/50/0, 50/45/5 and 50/40/10 biocomposites also present an endothermic peak at approximately 57 °C. The T_g of these biocomposites increased from 167 °C (100/0/0) to 195 °C (50/50/0) and approximately 172 °C (50/45/5 and 50/40/10), showing improved thermal stability conferred by CARSEP and MWCNT fillers. The DSC curve of CARSEP precursor shows an endothermic peak at 220 °C due to the decomposition of caramel, whereas the CARSEP filler presents improved thermal stability.

3.3. Morphological characterization by FESEM

The morphology of CARSEP precursor, CARSEP filler, and top and bottom surfaces of biocomposite films was investigated by FESEM, Fig. 5. The image of CARSEP precursor reveals aggregates of SEP fibers homogeneously covered by caramel (Fig. 5 A). The formation of aggregates is expected due to the drying step after ultrasonic homogenization. The image of CARSEP filler, obtained after pyrolysis of CARSEP precursor, shows aggregates of smaller size due to grinding and sieving (75 μm mesh). Additionally, the aggregates of SEP fibers are more exposed in CARSEP precursor (Fig. 5 A) than in the CARSEP filler due to the caramel decomposition during pyrolysis. (Fig. 5 F and K). The 100/0/0 film presents a smooth and continuous top and bottom surfaces (Fig. 5 B and G), whereas the cross-section shows small textural details resultant from the sample preparation for analysis (Fig. 5 L). The top, bottom, and cross-sectional images of the 50/50/0 film reveal a gravitational deposition of CARSEP particles, with larger particles predominantly settling on the bottom surface. This accumulation of particles disrupts the CS matrix network, leading to a heterogeneous surface (Fig. 5C–H and M). The top surface of 50/50/0 biocomposite (Fig. 5C), where Raman spectrum was acquired, is clearly dominated by CS, which explains the absence of CARSEP graphitic bands in this sample (Fig. 3B). The top, bottom, and cross-sectional images of 50/45/5 and 50/40/10 biocomposites show a more homogeneous distribution of particles (Fig. 5D–I, N, E, J, and O). This effect was promoted by the introduction of MWCNT into the system, since 510% CARSEP was replaced by MWCNT. However, MWCNT cannot be distinguished from CARSEP filler within CS matrix. Overall, the preparation of biocomposites by solvent casting leads to the gravitational deposition of CARSEP filler with an apparent weight gradient in the vertical direction *i.e.*, smaller aggregates on top surface and larger aggregates on the bottom. The introduction of MWCNT seems to attenuate this effect, contributing to a more homogeneous topography. The positive effect promoted by MWCNT in CS-based composites is described in literature. The combination of 2D montmorillonite clay platelets and 1D MWCNT create a 3D network that reinforce the interactions with CS matrix [51]. The same effect was observed for CS-based biocomposites containing rGO and MWCNT. In this later case, non-covalent π–π interactions between rGO and MWCNT are also expected to occur between CARSEP and MWCNT [52].

3.4. Mechanical properties

The stress strain curves, tensile strength, Young's modulus, and elongation at break of biocomposites films are displayed in Fig. 6. The biocomposite films present a thickness between 120 and 146 μm,

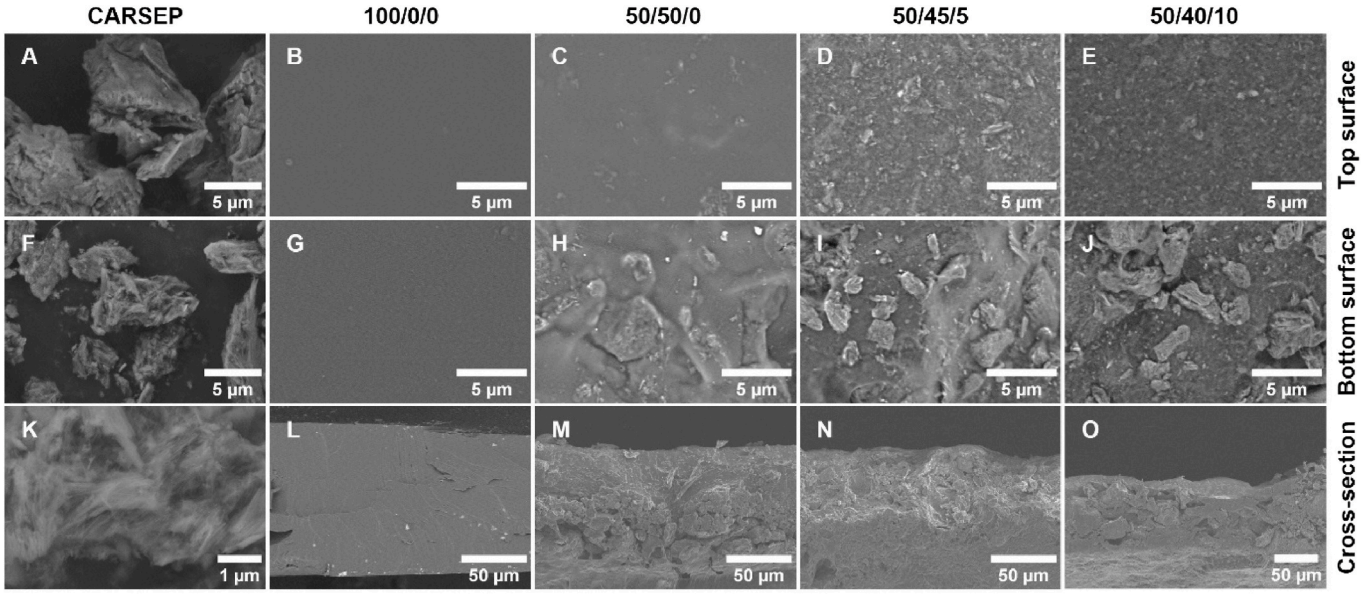

Fig. 5. FESEM images of (**A**) CARSEP precursor, (**F, K**) CARSEP filler, (**B–E**) top surface, (**G–J**) bottom surface and (**L–O**) cross section of 100/0/0, 50/50/0, 50/45/5, and 50/40/10 biocomposites, respectively.

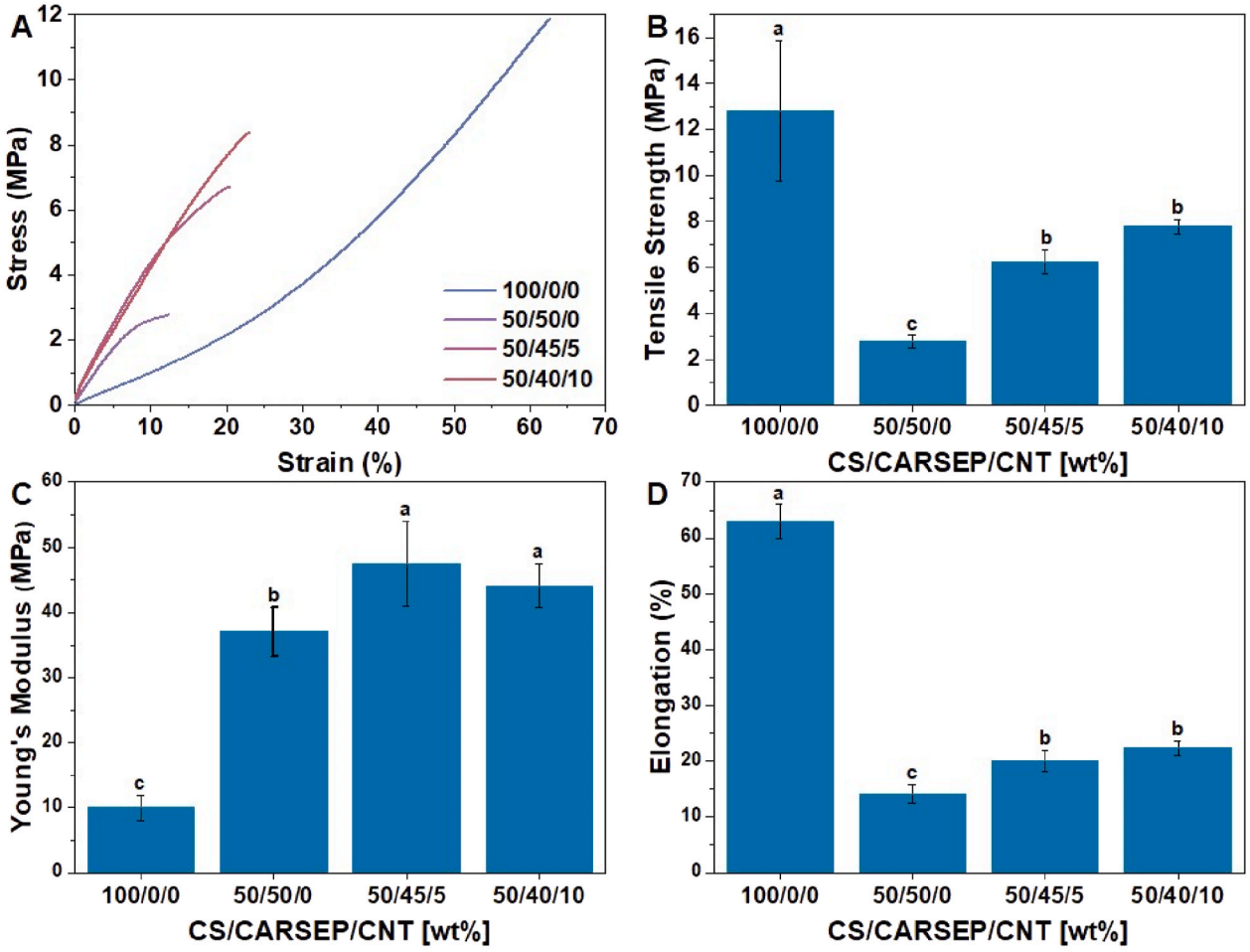

Fig. 6. Stress strain curves (**A**), tensile strength (**B**), Young's modulus (**C**), and elongation at break (**D**) of biocomposite films. Different letters (a, b, c) above error bars indicate statistical differences, $p < 0.05$. The error bars represent the standard deviation (n = 5).

Table 1. The tensile strength of CS film decreased from 13 MPa to 3 MPa with the incorporation of CARSEP filler (50/50/0), revealing a decrease in the mechanical resistance probably due to the decrease of interaction between the CS chains by the presence of the filler. On the other hand, this parameter increased up to 8 MPa when 5–10 wt% of CARSEP filler was replaced by MWCNT pointing a reinforcement of mechanical resistance, Fig. 6B.

The Young's modulus, measurement of non-permanent elastic deformation, increased with the incorporation of fillers from 10 MPa in 100/0/0 film, to a maximum of 48 MPa in 50/45/5 biocomposite, indicating an increase of films rigidity, Fig. 6C. The elongation at break decreased with the incorporation of fillers, from 63 % in 100/0/0 film to a minimum of 14% in 50/50/0 biocomposite. Although, similarly to the mechanical resistance, the flexibility was also enhanced by the MWCNT, Fig. 6D. In general, the mechanical properties of 100/0/0 CS film were strongly impacted when 50 wt% CS mass was replaced by an equal amount of CARSEP filler. In our previous works, biocomposites containing up to 50% rGO or 50 % rGO-$Fe_{3-x}O_4$ (both in relation to CS mass) showed an increase of tensile strength and Young's modulus and a decrease of elongation in comparison with the CS film [24,53]. The higher load and different nature of carbonaceous fillers used in the present work are the main factors behind the different mechanical behavior. Regarding the high load of CARSEP filler used here, it is expected to create a significant CARSEP-CARSEP network that disrupts the CS-CS network. The presence of aggregates, observed in SEM images, also causes discontinuities in the CS matrix, resulting in reduction of resistance and increased rigidity [54]. A significant improvement of mechanical properties is observed when 5–10 wt% of CARSEP filler is replaced by MWCNT, which is ascribed to the synergetic effect between the 1D and 2D fillers. These results confirm the improved homogeneity promoted by MWCNT as previously discussed in the SEM section. The mechanical properties of CS-based biocomposites containing montmorillonite or rGO, were greatly improved by MWCNT in comparison to the biocomposites containing single components [51,52]. The reinforcement of mechanical properties due to these synergetic effects would be higher if lower amounts of fillers were used. Nevertheless, the high load of CARSEP is mandatory to improve the electrical properties, which is the main scope of this work.

3.5. *Wettability, swelling and water solubility*

The wettability was determined by static water contact angle measurements, displacing 3 μL drops of ultrapure water on the top and bottom surfaces of biocomposite films, Table 2. The 100/0/0 film displays a hydrophobic top surface and a hydrophilic bottom surface, with contact angles of 98° and 43°, respectively. The hydrophobic nature of top surface of 100/0/0 is in good agreement with the values previously reported [24,55,56]. The big difference between the surfaces arises from the gravitational deposition of glycerol (hydrophilic), used as plasticizer, on the bottom of film during the solvent casting process. The 50/50/0, 50/45/5, and 50/40/10 biocomposites display hydrophilic surfaces with contact angles between 32 and 18°. The top surface of 50/50/0 film presents the highest contact angle (32°), since this surface is predominantly dominated by CS as observed in the SEM images. The

Table 2
Water contact angle (WCA), moisture, water swelling, and water solubility determined by weight loss percentage of CS/CARSEP/CNT biocomposite films. Different superscript letters (a, b, c, d) indicate statistical differences, $p < 0.05$.

Film	WCA [°]		Moisture [%]	Swelling [%]	Weight loss [%]
	Top	Bottom			
100/0/0	97.8 ± 1.8[a]	43.3 ± 4.1[b]	36.3 ± 2.5[a]	411.8 ± 32.8[a]	47.4 ± 2.3[a]
50/50/0	32.3 ± 1.8[c]	20.6 ± 3.2[d]	29.8 ± 2.4[b]	35.7 ± 11.9[b]	42.3 ± 1.7[b]
50/45/5	21.9 ± 0.7[d]	17.9 ± 2.0[d]	28.5 ± 0.7[b]	25.78 ± 3.8[b]	37.2 ± 2.0[b]
50/40/10	18.4 ± 1.0[d]	18.0 ± 1.7[d]	31.9 ± 2.1[a, b]	14.7 ± 4.6[b]	38.3 ± 0.4[b,c]

Results are presented as average value ± standard deviation (WCA: n = 15, Swelling and solubility: n = 3). Different superscript letters indicate statistical differences ($p < 0.05$).

bottom surface of 50/50/0 film shows a contact angle (21°) lower than top surface, as observed for 100/0/0. The contact angle of the different surfaces of 50/45/5 (top: 22°, bottom: 18°) and 50/40/10 (top: 18°, bottom: 18°) biocomposites becomes identical, confirming the improved homogeneity of biocomposites promoted by MWCNT. The hydrophobic top surface of CS becomes hydrophilic with the incorporation of CARSEP filler. Nevertheless, the carbon covering the surface of SEP is expected to be hydrophobic [40]. Additionally, the CS-rGO biocomposites previously reported by us, showed contact angles between 66 and 78° [24]. The roughness of biocomposites surfaces caused by the fillers might be responsible for the higher hydrophilicity. The CARSEP filler exposed at the surfaces might display air filled protrusions responsible to adsorb the water droplets, as observed for the biohybrid films containing halloysite, SEP and cellulose nanofibers [42].

The 100/0/0 film presents a swelling of 412% that was drastically reduced in the case of biocomposites, Table 2. The swelling in water depends on the availability of hydrophilic groups to interact with water molecules. In the case of 100/0/0 film, the hydroxyl and amine groups of CS are available to establish interactions with water leading to the swollen state [57]. The biocomposites 50/50/0, 50/45/5, and 50/40/10 present swelling values of 36, 26 and 15%, respectively. The biocomposites are composed of 50 wt% CS and 50 wt% carbon fillers, but the swelling percentage of biocomposites is lower than half of swelling percentage of 100/0/0 film, decreasing even more with the increasing concentration of MWCNT. These results also support the establishment of chemical interactions between the CS matrix and carbon fillers, turning the hydrophilic functional groups of CS unavailable to interact with water. This effect is reinforced in the presence of MWCNT, as previously suggested by SEM images, mechanical properties, and water contact angle results. The same effect was observed for the swelling of CS hydrogels that was also reduced from 107 to 28% with the incorporation of GO that presented a crosslinking effect [57].

The water solubility of biocomposites was determined after keeping the films submerged in water under constant stirring for seven days, Table 2. The weight loss of 100/0/0, 50/50/0, 50/45/5, and 50/40/10 biocomposites was 47, 42, 37 and 38%, respectively. The 100/0/0 film solubility was reduced by the addition of carbonaceous fillers. The water solubility is attributed to the diffusion of glycerol to water [58]. There was no apparent degradation of films or visible separated black particles after the seven days immersed in water. The reduction of CS water solubility in presence of carbonaceous fillers also occurred in CS biocomposites containing rGO or rGO-$Fe_{3-x}O_4$ [24,53].

3.6. Electrical conductivity of biocomposite films

The electrical conductivity of biocomposites was investigated by *dc* measurements in-plane and through-plane directions, Fig. 7. The 100/0/0 film is an electrical insulator and the introduction of CARSEP into CS,

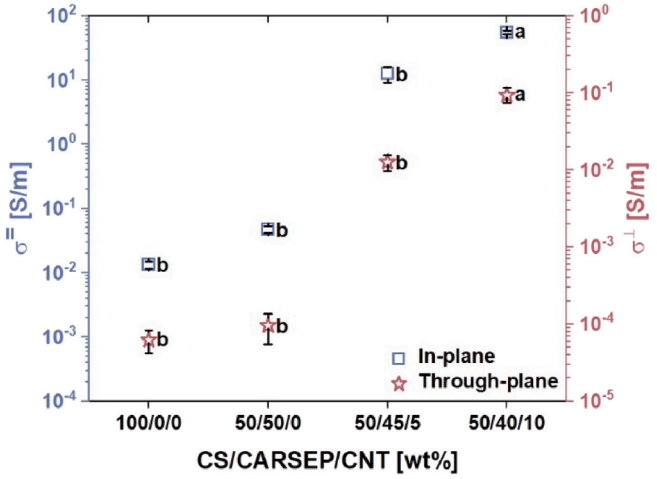

Fig. 7. Electrical conductivity of biocomposite films in-plane and through-plane directions. Different letters (a, b) indicate statistical differences, $p < 0.05$. The error bars represent the standard deviation (n = 3).

50/50/0 biocomposite, did not significantly improve the electrical conductivity. The incorporation of MWCNT to CS matrix revealed to be the most important parameter to enhance the electrical conductivity by three orders of magnitude in both directions, reaching a maximum of 55.5 S/m (in-plane) and 0.1 S/m (through-plane) in the case of 50/40/10 film.

The in-plane electrical conductivity reported here is considerably high in comparison with similar biocomposites reported in literature, especially considering the lower amount of electrically conductivity filler, Fig. 8. To the best of our knowledge, the only two works that reported superior in-plane electrical conductivity in the range of 10^3 S/m contained higher loads of conductive fillers. One study is related to biocomposites of cellulose containing 22.7 wt% MWCNT [59], and the other one to biocomposites of alginate/SEP containing 55.6 wt% GNP (12000 S/m) and 10 % MWCNT in relation to GNP content [31].

Few works report the through-plane electrical conductivity. However, this property is very relevant for applications where the electrical current needs to cross the material *e.g.,* piezoresistive sensors or electrically conductive packaging. In the latter case, the in-pack food sterilization by PEF, requires the passage of electrical current through the packaging to reach the packed food. The electrical conductivity of food

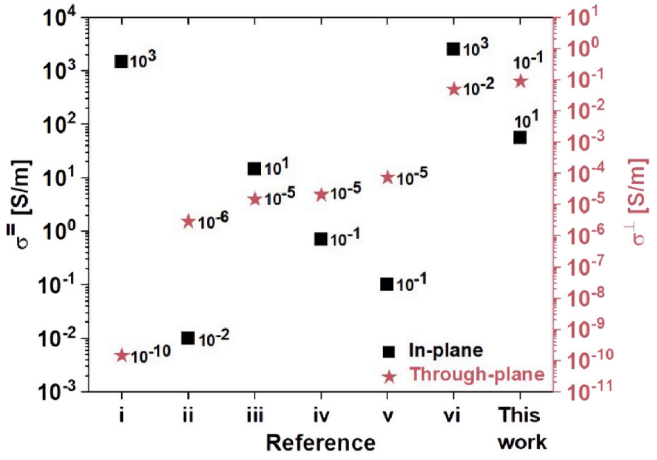

Fig. 8. Comparison of electrical conductivity of 50/40/10 chitosan-based biocomposite (this work) with other biocomposites reported in literature: **i.** Cellulose/22.7 wt% MWCNT [59], **ii.** Starch/25 % rGO [60], **iii.** Starch/5 % MWCNT [25], **iv.** CS/50 % rGO [24], **v.** Alginate/50 % ZnO-rGO [61], **vi.** Alginate/55.6 % GNP/10 % MWCNT [31].

is typically between 0.1 and 2 S/m. Therefore, the through-plane electrical conductivity of the packaging should match these values [19]. In this work, the through-plane electrical conductivity of 50/40/10 film (0.1 S/m) meets this criterion, highlighting its potential for this application. However, this is just an example of a wide range of possible applications of this material. The electrical conductivity in-plane is higher than through-plane direction, which is in good agreement with other works reported in literature, Fig. 8. The isotropic electrical conductivity in films of carbon-based composites remains a challenge. The carbonaceous fillers have a preferential alignment in-plane direction, creating a percolation network in this direction rather than through-plane [24–26,31,60,61]. In 50/40/10 biocomposite, the difference between in-plane and through-plane conductivities is only of three orders of magnitude, being the lowest difference among other works, Fig. 8. This achievement is facilitated by the use of a multicomponent filler system, CARSEP and MWCNT, instead of a single filler component. CARSEP filler creates excluded volume that increases the probability of MWCNT being interconnected [62] and their possible orientation in-plane and through-plane directions, as schematically represented in Fig. 9. The micrometric size and high load of CARSEP are the main factors promoting this effect. If nanometric particles and/or low loads were used, the MWCNT would aggregate, and the percolation network would be reduced [63]. Therefore, the use of CARSEP combined with MWCNT was the key parameter to achieve significant through-plane electrical conductivity.

Overall, the high filler loads necessary to achieve the through-plane electrical conductivity reported here simultaneously affect other material properties. The increased filler content enhances thermal stability and reduces swelling and water solubility. However, these improvements come at the cost of mechanical strength, flexibility, and increased surface hydrophilicity. Therefore, the future design of electrically conductive biocomposites should carefully balance these effects according to the specific applications.

3.7. Migration study

The 50/40/10 biocomposite film presented the highest electrical conductivity in-plane and through-plane directions, which is a relevant property for many practical applications. The contact of the film with liquids is a predictable scenario in diverse applications, *e.g.*, food packaging, biotechnology or the biomedical fields [5,64,65]. The potential release of compounds from the biocomposite in dry and wet state can compromise the application, especially if placed in contact with food or cells. Therefore, a migration study was performed to detect the compounds released from the biocomposite in three different simulants air, ethanol, and hexane, after heating at 60 °C for 1 h. Ethanol and hexane were selected as solvents due to their distinct polarities, covering the migration of compounds from the biocomposite to a wide range of mediums. The volatile compounds were analyzed by GC-MS, Fig. 10. The chromatogram of the head-space from the vial after film heating shows the absence of released compounds, Fig. 10A. The chromatogram of ethanol extract (Fig. 10B), as well as the homologous sample concentrated under nitrogen flow (Fig. 10C) only reveal the presence of glycerol (CAS 56-81-5). The injection of an internal standard allowed the semi-quantification of glycerol, determined to be 9.11 mg/L. The chromatogram of hexane extract (Fig. 10D), and the respective concentrated sample (Fig. 10E), do not indicate the presence of any compound. The release of glycerol to water was mentioned above as the main factor contributing to the water solubility of films. Therefore, the migration of glycerol to other polar solvents such as ethanol was expected. The amount of glycerol estimated to be released to ethanol is less than 1 % of total glycerol incorporated. The water solubility of this film was 38.3 ± 0.4 %. The difference in glycerol migration in both cases is mainly attributed to different contact times of film with solvents *i.e.*, 1 h of contact with ethanol and 7 days of contact with water. On the other hand, glycerol is insoluble in apolar compounds such hexane not being released to this solvent. Glycerol is a non-toxic compound, here used as plasticizer, being even allowed as food additive with an allowed daily intake of 2 g kg^{-1} day^{-1} [13,66]. The absence of toxic compounds released by the biocomposite paves the way for its safe application in several fields.

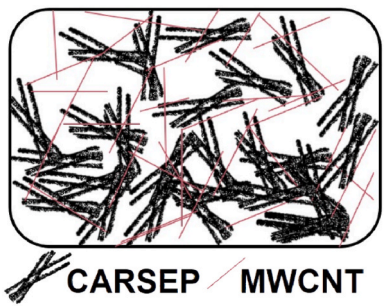

Fig. 9. Schematic representation of CARSEP and interconnected MWCNT distribution in CS matrix.

4. Conclusions

Electrically conductive biocomposite films containing CS matrix and CARSEP with MWCNT fillers were developed. The structural characterization of CARSEP filler by XRD, solid-state ^{13}C CP MAS-NMR and Raman confirmed the conversion of caramel into a carbonaceous material after pyrolysis. The incorporation of CARSEP and MWCNT in the CS matrix improved the thermal stability and water solubility of CS films, while the swelling percentage was drastically reduced. The use of a carbonaceous multicomponent filler system improved the homogenous distribution of MWCNT in different directions. This strategy enhanced the challenging through-plane electrical conductivity of biocomposite films by three orders of magnitude. The 50/40/10 biocomposite achieved a through-plane electrical conductivity of 0.1 S/m, matching the value required for materials to be used for in-pack food sterilization by PEF. The maximum in-plane electrical conductivity of 55.5 S/m is also relevant, considering the lower amount of MWCNT in comparison with similar biocomposites reported in literature. The migration study performed using solvents with distinct polarities demonstrated that no harmful compounds are released when this biocomposite film is heated up to 60 °C. The combination of flexibility, electrical conductivity and a biopolymer-based matrix is attractive for the application of biocomposites in packaging, electronics, or biomedical field.

CRediT authorship contribution statement

Ana Barra: Writing – original draft, Methodology, Investigation, Formal analysis, Data curation, Conceptualization. **Nuno M. Ferreira:** Writing – review & editing, Formal analysis, Data curation. **Fátima Poças:** Writing – review & editing, Formal analysis, Data curation. **Eduardo Ruiz-Hitzky:** Writing – review & editing, Supervision, Methodology, Conceptualization. **Cláudia Nunes:** Writing – review & editing, Writing – original draft, Supervision, Methodology, Conceptualization. **Paula Ferreira:** Writing – review & editing, Writing – original draft, Validation, Supervision, Project administration, Methodology, Investigation, Conceptualization.

Data availability

Data generated or analyzed during this study are provided in full within the published article and its supplementary materials.

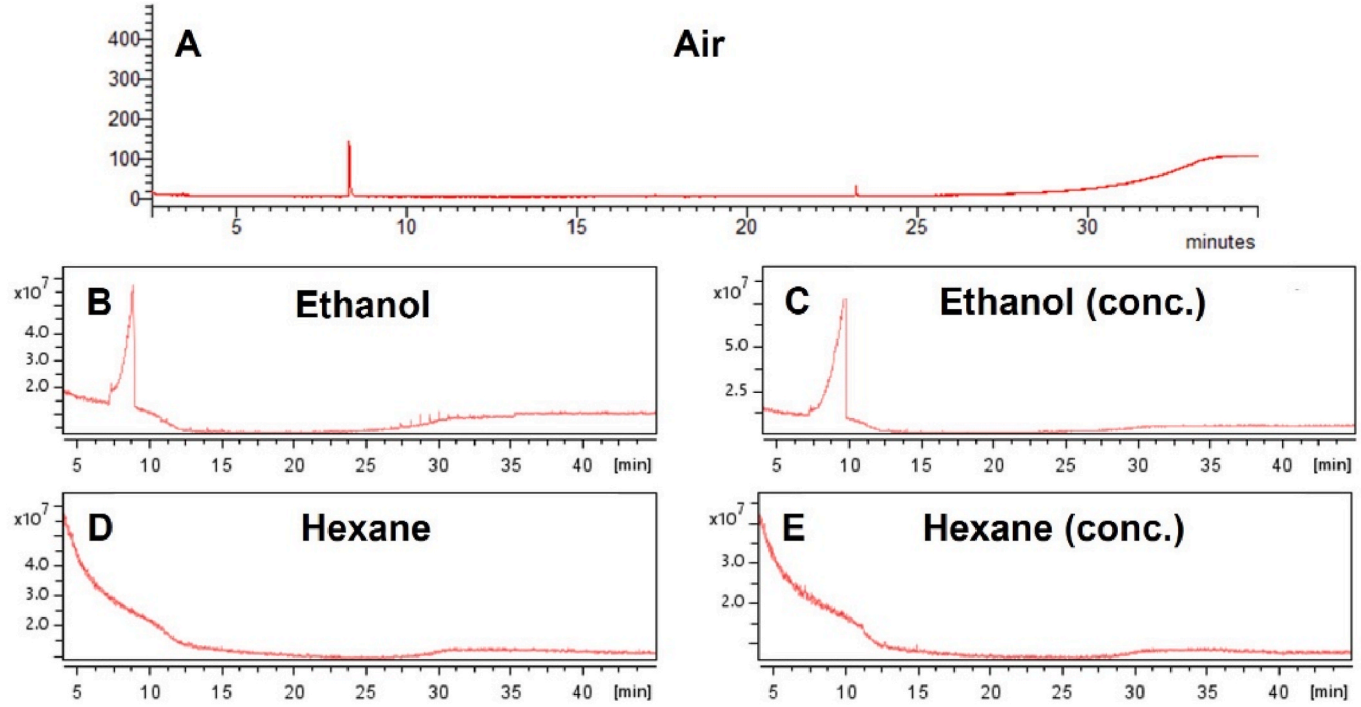

Fig. 10. GC-MS chromatograms of different extracts of 50/40/10 after heating at 60 °C for 1h (**A**) air, (**B**) ethanol, (**C**) concentrated ethanol, (**D**) hexane and (**E**) concentrated hexane.

Declaration of competing interest

The authors declare the following financial interests/personal relationships which may be considered as potential competing interests: Paula Ferreira reports financial support was provided by Foundation for Science and Technology. If there are other authors, they declare that they have no known competing financial interests or personal relationships that could have appeared to influence the work reported in this paper.

Acknowledgments

This work was developed within the scope of the project CICECO - Aveiro Institute of Materials, UIDB/50011/2020, UIDP/50011/2020 & LA/P/0006/2020, i3N (LA/P/0037/2020, UIDB/50025/2020 and UIDP/50025/2020), and CBQF (UIDB/50016/2020) financed by national funds through the FCT/MCTES (PIDDAC). AB is thankful to FCT for grant SFRH/BD/148856/2019. CN is grateful to Portuguese national funds (OE), through FCT, I.P., in the scope of the framework contract foreseen in the numbers 4, 5 and 6 of the article 23, of the Decree-Law 57/2016, of August 29, changed by Law 57/2017, of July 19 (DL 57/2016/CP1482/CT0031). ERH: acknowledge financial support from the MCIN/AEI/10.13039/501100011033 (Spain, project PID2019-105479RB-I00).

References

[1] J. Ouyang, Application of intrinsically conducting polymers in flexible electronics, SmartMat 2 (3) (2021) 263–285, https://doi.org/10.1002/smm2.1059.
[2] T. Nezakati, A. Seifalian, A. Tan, A.M. Seifalian, Conductive polymers: opportunities and challenges in biomedical applications, Chem. Rev. 118 (14) (2018) 6766–6843, https://doi.org/10.1021/acs.chemrev.6b00275.
[3] M.R. Chia, S.W. Phang, I. Ahmad, Emerging applications of versatile polyaniline-based polymers in the food industry, Polymers (Basel) 14 (23) (2022), https://doi.org/10.3390/polym14235168.
[4] P. Cataldi, L. Ceseracciu, A. Athanassiou, I.S. Bayer, Healable cotton-graphene nanocomposite conductor for wearable electronics, ACS Appl. Mater. Interfaces 9 (16) (2017) 13825–13830, https://doi.org/10.1021/acsami.7b02326.
[5] A.M. Martins, G. Eng, S.G. Caridade, J.F. Mano, R.L. Reis, G. Vunjak-Novakovic, Electrically conductive chitosan/carbon scaffolds for cardiac tissue engineering, Biomacromolecules 15 (2014) 635–643, https://doi.org/10.1021/bm401679q.
[6] P. Cataldi, L. Lamanna, C. Bertei, F. Arena, P. Rossi, M. Liu, F. Di Fonzo, D. G. Papageorgiou, A. Luzio, M. Caironi, An electrically conductive oleogel paste for edible electronics, Adv. Funct. Mater. 32 (23) (2022), https://doi.org/10.1002/adfm.202113417.
[7] P. Rozhin, S. Adorinni, D. Iglesias, T. Mackiol, S. Kralj, M. Bisetto, M. Abrami, M. Grassi, M. Bevilacqua, P. Fornasiero, S. Marchesan, Nanocomposite hydrogels with self-assembling peptide-functionalized carbon nanostructures, Chem. Eur J. 29 (71) (2023) 1–7, https://doi.org/10.1002/chem.202301708.
[8] S. Islam, M.A.R. Bhuiyan, M.N. Islam, Chitin and chitosan: structure, properties and applications in biomedical engineering, J. Polym. Environ. 25 (3) (2017) 854–866, https://doi.org/10.1007/s10924-016-0865-5.
[9] L. Zhao, N. Baccile, S. Gross, Y. Zhang, W. Wei, Y. Sun, M. Antonietti, M.M. Titirici, Sustainable nitrogen-doped carbonaceous materials from biomass derivatives, Carbon N. Y. 48 (13) (2010) 3778–3787, https://doi.org/10.1016/j.carbon.2010.06.040.
[10] D. Zhao, S. Yu, B. Sun, S. Gao, S. Guo, K. Zhao, Biomedical applications of chitosan and its derivative nanoparticles, Polymers (Basel) 10 (4) (2018) 1–17, https://doi.org/10.3390/polym10040462.
[11] R. Priyadarshi, J.W. Rhim, Chitosan-based biodegradable functional films for food packaging applications, Innov. Food Sci. Emerg. Technol. 62 (2020) 1–20, https://doi.org/10.1016/j.ifset.2020.102346.
[12] C. Wang, T. Yokota, T. Someya, Natural biopolymer-based biocompatible conductors for stretchable bioelectronics, Chem. Rev. 121 (4) (2021) 2109–2146, https://doi.org/10.1021/acs.chemrev.0c00897.
[13] A.S. Sharova, F. Modena, A. Luzio, F. Melloni, P. Cataldi, F. Viola, L. Lamanna, N. F. Zorn, M. Sassi, C. Ronchi, J. Zaumseil, L. Beverina, M.R. Antognazza, M. Caironi, Chitosan-gated organic transistors printed on ethyl cellulose as a versatile platform for edible electronics and bioelectronics, Nanoscale (2023), https://doi.org/10.1039/D3NR01051A.
[14] S.J. Paul, I. Sharma, I. Elizabeth, B. Gahtori, R. Manikandan, S.S. Titus, P. Chandra, B.K. Gupta, A comparative study of compressible and conductive vertically aligned carbon nanotube forest in different polymer matrixes for high-performance piezoresistive force sensors, ACS Appl. Mater. Interfaces 12 (14) (2020) 16946–16958, https://doi.org/10.1021/acsami.0c01779.
[15] N. Chikyu, T. Nakano, G. Kletetschka, Y. Inoue, Excellent electromagnetic interference shielding characteristics of a unidirectionally oriented thin multiwalled carbon nanotube/polyethylene film, Mater. Des. 195 (2020) 108918, https://doi.org/10.1016/j.matdes.2020.108918.
[16] A. Barra, J.D.C. Santos, M.R.F. Silva, C. Nunes, E. Ruiz-Hitzky, I. Gonçalves, S. Yildirim, P. Ferreira, P.A.A.P. Marques, Graphene derivatives in biopolymer-based composites for food packaging applications, Nanomaterials 10 (10) (2020) 2077, https://doi.org/10.3390/nano10102077.
[17] L. Guadagno, L. Vertuccio, F. Foglia, M. Raimondo, G. Barra, A. Sorrentino, R. Pantani, E. Calabrese, Flexible eco-friendly multilayer film heaters, Compos.

Part B Eng. 224 (July) (2021) 109208, https://doi.org/10.1016/j.compositesb.2021.109208.
[18] G. Ghoshal, Comprehensive review on pulsed electric field in food preservation: gaps in current studies for potential future research, Heliyon 9 (6) (2023) e17532, https://doi.org/10.1016/j.heliyon.2023.e17532.
[19] B. Roodenburg, S.W.H. de Haan, L.B.J. van Boxtel, V. Hatt, P.C. Wouters, P. Coronel, J.A. Ferreira, Conductive plastic film electrodes for pulsed electric field (PEF) treatment-A proof of principle, Innov. Food Sci. Emerg. Technol. 11 (2) (2010) 274–282, https://doi.org/10.1016/j.ifset.2010.01.005.
[20] K. Ahmed, M. Hasan, J. Haider, Electrical and mechanical properties of sugarcane bagasse pyrolyzed biochar reinforced polyvinyl alcohol biocomposite films, J. Compos. Sci. 5 (9) (2021) 1–14, https://doi.org/10.3390/jcs5090249.
[21] J. Chen, H. Li, L. Zhang, C. Du, T. Fang, J. Hu, Direct reduction of graphene oxide/nanofibrillated cellulose composite film and its electrical conductivity research, Sci. Rep. 10 (1) (2020) 1–10, https://doi.org/10.1038/s41598-020-59918-z.
[22] H. Zhang, X. Sun, M.A. Hubbe, L. Pal, Highly conductive carbon nanotubes and flexible cellulose nano fibers composite membranes with semi-interpenetrating networks structure, Carbohydr. Polym. 222 (2019) 1–8, https://doi.org/10.1016/j.carbpol.2019.115013.
[23] Y. Zhan, C. Xiong, J. Yang, Z. Shi, Q. Yang, Flexible cellulose nanofibril/pristine graphene nanocomposite films with high electrical conductivity, Compos. Part A Appl. Sci. Manuf. 119 (January) (2019) 119–126, https://doi.org/10.1016/j.compositesa.2019.01.029.
[24] A. Barra, N.M. Ferreira, M.A. Martins, O. Lazar, A. Pantazi, A.A. Jderu, S. M. Neumayer, B.J. Rodriguez, M. Enăchescu, P. Ferreira, C. Nunes, Eco-friendly preparation of electrically conductive chitosan - reduced graphene oxide flexible bionanocomposites for food packaging and biological applications, Compos. Sci. Technol. 173 (November 2018) (2019) 53–60, https://doi.org/10.1016/j.compscitech.2019.01.027.
[25] Z. Alves, B. Abreu, N.M. Ferreira, E.F. Marques, C. Nunes, P. Ferreira, Enhancing the dispersibility of multiwalled carbon nanotubes within starch-based films by the use of ionic surfactants, Carbohydr. Polym. 273 (August) (2021), https://doi.org/10.1016/j.carbpol.2021.118531.
[26] N. Yousefi, M.M. Gudarzi, Q. Zheng, S.H. Aboutalebi, F. Sharif, J.-K. Kim, Self-alignment and high electrical conductivity of ultralarge graphene oxide–polyurethane nanocomposites, J. Mater. Chem. 22 (25) (2012) 12709–12717, https://doi.org/10.1039/c2jm30590a.
[27] S. Kim, S. Jung, W.J. Kim, Vertical alignment of carbon nanotubes in photo-curable polymer for multi-functional hybrid materials, Appl. Surf. Sci. 612 (September 2022) (2023) 155749, https://doi.org/10.1016/j.apsusc.2022.155749.
[28] G. Wang, M. Zheng, Z. Liu, M. Wang, Anisotropic piezoresistive sensors made with magnetically induced vertically aligned carbon nanotubes/polydimethylsiloxane, ACS Appl. Mater. Interfaces 15 (2023) 51675–51683, https://doi.org/10.1021/acsami.3c09104.
[29] M. Raimondo, G. Donati, G. Milano, L. Guadagno, Hybrid composites based on carbon nanotubes and graphene nanosheets outperforming their single-nanofiller counterparts, FlatChem 36 (August) (2022) 100431, https://doi.org/10.1016/j.flatc.2022.100431.
[30] X. Luo, G. Yang, D.W. Schubert, Electrically conductive polymer composite containing hybrid graphene nanoplatelets and carbon nanotubes: synergistic effect and tunable conductivity anisotropy, Adv. Compos. Hybrid Mater. 5 (1) (2022) 250–262, https://doi.org/10.1007/s42114-021-00332-y.
[31] E. Ruiz-Hitzky, M.M.C. Sobral, A. Gómez-Avilés, C. Nunes, C. Ruiz-García, P. Ferreira, P. Aranda, Clay-graphene nanoplatelets functional conducting composites, Adv. Funct. Mater. 26 (41) (2016) 7394–7405, https://doi.org/10.1002/adfm.201603103.
[32] E. Ruiz-Hitzky, Molecular access to intracrystalline tunnels of sepiolite, J. Mater. Chem. 11 (1) (2001) 86–91, https://doi.org/10.1039/b003197f.
[33] A.I. Ruiz, C. Ruiz-García, E. Ruiz-Hitzky, From old to New inorganic materials for advanced applications: the paradigmatic example of the sepiolite clay mineral, Appl. Clay Sci. 235 (2023) 106874, https://doi.org/10.1016/J.CLAY.2023.106874.
[34] E. Ruiz-Hitzky, C. Ruiz-García, F.M. Fernandes, G. Lo Dico, L. Lisuzzo, V. Prevot, M. Darder, P. Aranda, Sepiolite-hydrogels: synthesis by ultrasound irradiation and their use for the preparation of functional clay-based nanoarchitectured materials, Front. Chem. 9 (2021) 657, https://doi.org/10.3389/FCHEM.2021.733105/BIBTEX.
[35] E. Ruiz-Hitzky, P. Aranda, A. Álvarez, J. Santarén, A. Esteban-Cubillo, Chapter 17 - advanced materials and New applications of sepiolite and palygorskite, in: E. Galán, A. Singer (Eds.), Developments in Clay Science, Elsevier, 2011, pp. 393–452.
[36] M. Darder, M. López-Blanco, P. Aranda, A.J. Aznar, J. Bravo, E. Ruiz-Hitzky, Microfibrous Chitosan–Sepiolite nanocomposites, Chem. Mater. 18 (6) (2006) 1602–1610, https://doi.org/10.1021/cm0523642.
[37] A. Barra, O. Lazăr, G. Mihai, C. Bratu, C. Ruiz-García, M. Darder, P. Aranda, M. Enăchescu, C. Nunes, P. Ferreira, E. Ruiz-Hitzky, Graphene-like materials supported on sepiolite clay synthesized at relatively low temperature, Carbon N. Y. 218 (2024) 118767, https://doi.org/10.1016/j.carbon.2023.118767. November 2023.
[38] C. Ruiz-García, M. Darder, P. Aranda, E. Ruiz-Hitzky, Toward a green way for the chemical production of supported graphenes using porous solids, J. Mater. Chem. A 2 (7) (2017) 2009–2017, https://doi.org/10.1039/c3ta13716c.
[39] E. Ruiz-Hitzky, M. Darder, F.M. Fernandes, E. Zatile, F.J. Palomares, P. Aranda, Supported graphene from natural resources: easy preparation and applications, Adv. Mater. 23 (44) (2011) 5250–5255, https://doi.org/10.1002/adma.201101988.
[40] C. Ruiz-García, J. Pérez-Carvajal, A. Berenguer-Murcia, M. Darder, P. Aranda, D. Cazorla-Amorós, E. Ruiz-Hitzky, Clay-supported graphene materials: application to hydrogen storage, Phys. Chem. Chem. Phys. 15 (42) (2013) 18635–18641, https://doi.org/10.1039/c3cp53258e.
[41] W. Yin, M. Liu, Y.Y. Chen, Q.Z. Yao, S.Q. Fu, G.T. Zhou, Microwave-assisted preparation of Mn3O4@sepiolite nanocomposite for highly efficient removal of uranium, Appl. Clay Sci. 228 (April) (2022) 106597, https://doi.org/10.1016/j.clay.2022.106597.
[42] L. Lisuzzo, B. Wicklein, G. Lo Dico, G. Lazzara, G. Del Real, P. Aranda, E. Ruiz-Hitzky, Functional biohybrid materials based on halloysite, sepiolite and cellulose nanofibers for health applications, Dalt. Trans. 49 (12) (2020) 3830–3840, https://doi.org/10.1039/C9DT03804C.
[43] R. Fernández-Saavedra, P. Aranda, E. Ruiz-Hitzky, Templated synthesis of carbon nanofibers from polyacrylonitrile using sepiolite, Adv. Funct. Mater. 14 (1) (2004) 77–82, https://doi.org/10.1002/adfm.200305514.
[44] C. Nunes, É. Maricato, Â. Cunha, M.A.M. Rocha, S. Santos, P. Ferreira, M.A. Silva, A. Rodrigues, O. Amado, J. Coimbra, D. Silva, A. Moreira, S. Mendo, J.A. Lopes Da Silva, E. Pereira, S.M. Rocha, M.A. Coimbra, Chitosan-genipin film, a sustainable methodology for wine preservation, Green Chem. 18 (19) (2016) 5331–5341, https://doi.org/10.1039/c6gc01621a.
[45] Y. Pan, T. Wu, H. Bao, L. Li, Green fabrication of chitosan films reinforced with parallel aligned graphene oxide, Carbohydr. Polym. 83 (4) (2011) 1908–1915, https://doi.org/10.1016/j.carbpol.2010.10.054.
[46] C. Falco, F.P. Caballero, F. Babonneau, C. Gervais, G. Laurent, M.-M. Titirici, N. Baccile, Hydrothermal carbon from biomass: structural differences between hydrothermal and pyrolyzed carbons via 13C solid state NMR, Langmuir 27 (2011) 14460–14471.
[47] M. Darder, E. Ruiz-Hitzky, Caramel-clay nanocomposites, J. Mater. Chem. 15 (35–36) (2005) 3913–3918, https://doi.org/10.1039/b505958e.
[48] J. Xu, Q. He, Z. Xiong, Y. Yu, S. Zhang, X. Hu, L. Jiang, S. Su, S. Hu, Y. Wang, J. Xiang, Raman spectroscopy as a versatile tool for investigating thermochemical processing of coal, biomass, and wastes: recent advances and future perspectives, Energy Fuel. 35 (4) (2021) 2870–2913, https://doi.org/10.1021/ACS.ENERGYFUELS.0C03298/ASSET/IMAGES/LARGE/EF0C03298_0025.JPEG.
[49] S.M. Costa, D.P. Ferreira, P. Teixeira, L.F. Ballesteros, J.A. Teixeira, R. Fangueiro, Active natural-based films for food packaging applications: the combined effect of chitosan and nanocellulose, Int. J. Biol. Macromol. 177 (2021) 241–251, https://doi.org/10.1016/j.ijbiomac.2021.02.105.
[50] J. Zawadzki, H. Kaczmarek, Thermal treatment of chitosan in various conditions, Carbohydr. Polym. 80 (2) (2010) 394–400, https://doi.org/10.1016/j.carbpol.2009.11.037.
[51] C. Tang, L. Xiang, J. Su, K. Wang, C. Yang, Q. Zhang, Q. Fu, Largely improved tensile properties of chitosan film via unique synergistic reinforcing effect of carbon nanotube and clay, J. Phys. Chem. B 112 (13) (2008) 3876–3881, https://doi.org/10.1021/jp709977m.
[52] Y. Pan, H. Bao, L. Li, Noncovalently functionalized multiwalled carbon nanotubes by chitosan-grafted reduced graphene oxide and their synergistic reinforcing effects in chitosan films, ACS Appl. Mater. Interfaces 3 (12) (2011) 4819–4830, https://doi.org/10.1021/am2013135.
[53] A. Barra, Z. Alves, N.M. Ferreira, M.A. Martins, H. Oliveira, L.P. Ferreira, M. M. Cruz, M. de D. Carvalho, S.M. Neumayer, B.J. Rodriguez, C. Nunes, P. Ferreira, Biocompatible chitosan-based composites with properties suitable for hyperthermia therapy, J. Mater. Chem. B 8 (6) (2020) 1256–1265, https://doi.org/10.1039/C9TB02067E.
[54] G. Lo Dico, B. Wicklein, L. Lisuzzo, G. Lazzara, P. Aranda, E. Ruiz-Hitzky, Multicomponent bionanocomposites based on clay nanoarchitectures for electrochemical devices, Beilstein J. Nanotechnol. 10 (2019) 1303–1315, https://doi.org/10.3762/BJNANO.10.129.
[55] A.S. Ferreira, C. Nunes, A. Castro, P. Ferreira, M.a. Coimbra, Influence of grape pomace extract incorporation on chitosan films properties, Carbohydr. Polym. 113 (2014) 490–499, https://doi.org/10.1016/j.carbpol.2014.07.032.
[56] C. Nunes, É. Maricato, Â. Cunha, A. Nunes, J. a L. da Silva, M.a. Coimbra, Chitosan-caffeic acid-genipin films presenting enhanced antioxidant activity and stability in acidic media, Carbohydr. Polym. 91 (1) (2013) 236–243, https://doi.org/10.1016/j.carbpol.2012.08.033.
[57] B. Li, J. Wang, Q. Gui, H. Yang, Drug-loaded chitosan film prepared via facile solution casting and air-drying of plain water-based chitosan solution for ocular drug delivery, Bioact. Mater. 5 (3) (2020) 577–583, https://doi.org/10.1016/j.bioactmat.2020.04.013.
[58] I. Gonçalves, C. Nunes, S. Mendes, L.O. Martins, P. Ferreira, M.A. Coimbra, CotA laccase-ABTS/hydrogen peroxide system: an efficient approach to produce active and decolorized chitosan-genipin films, Carbohydr. Polym. 175 (2017) 628–635, https://doi.org/10.1016/j.carbpol.2017.08.029.
[59] H. Lu, Z. Xia, X. Zheng, Q. Mi, J. Zhang, Y. Zhou, C. Yin, J. Zhang, Patternable cellulose/MWCNT laminated nanocomposites with anisotropic thermal and electrical conductivity, Compos. Commun. 26 (April) (2021) 100786, https://doi.org/10.1016/j.coco.2021.100786.
[60] Z. Alves, N.M. Ferreira, P. Ferreira, C. Nunes, Design of heat sealable starch-chitosan bioplastics reinforced with reduced graphene oxide for active food packaging, Carbohydr. Polym. 291 (April) (2022), https://doi.org/10.1016/j.carbpol.2022.119517.
[61] Z. Alves, N.M. Ferreira, S. Mendo, P. Ferreira, C. Nunes, Design of alginate-based bionanocomposites with electrical conductivity for active food packaging, Int. J. Mol. Sci. 22 (18) (2021) 9943, https://doi.org/10.3390/IJMS22189943.

[62] H. Da Bao, Z.X. Guo, J. Yu, Effect of electrically inert particulate filler on electrical resistivity of polymer/multi-walled carbon nanotube composites, Polymer (Guildf). 49 (17) (2008) 3826–3831, https://doi.org/10.1016/j.polymer.2008.06.024.

[63] S.H. Park, J. Hwang, G.S. Park, J.H. Ha, M. Zhang, D. Kim, D.J. Yun, S. Lee, S. H. Lee, Modeling the electrical resistivity of polymer composites with segregated structures, Nat. Commun. 10 (1) (2019) 1–11, https://doi.org/10.1038/s41467-019-10514-4.

[64] B. Roodenburg, S.W.H. De Haan, J.A. Ferreira, P. Coronel, P.C. Wouters, V. Hatt, Toward 6 Log10 pulsed electric field inactivation with conductive plastic packaging material, J. Food Process. Eng. 36 (1) (2013) 77–86, https://doi.org/10.1111/j.1745-4530.2011.00655.x.

[65] S. Kim, L.K. Jang, M. Jang, S. Lee, J.G. Hardy, J.Y. Lee, Electrically conductive polydopamine-polypyrrole as high performance biomaterials for cell stimulation in vitro and electrical signal recording in vivo, ACS Appl. Mater. Interfaces 10 (39) (2018) 33032–33042, https://doi.org/10.1021/acsami.8b11546.

[66] A. Mortensen, F. Aguilar, R. Crebelli, A. Di Domenico, B. Dusemund, M.J. Frutos, P. Galtier, D. Gott, U. Gundert-Remy, J.C. Leblanc, O. Lindtner, P. Moldeus, P. Mosesso, D. Parent-Massin, A. Oskarsson, I. Stankovic, I. Waalkens-Berendsen, R. A. Woutersen, M. Wright, M. Younes, P. Boon, D. Chrysafidis, R. Güurtler, P. Tobback, A.M. Rincon, A. Tard, C. Lambrée, Re-evaluation of glycerol (E 422) as a food additive, EFSA J. 15 (3) (2017), https://doi.org/10.2903/J.EFSA.2017.4720.